Electric quadrupole strength in ^{20}Ne from the ^{19}F($\vec{p},\gamma_0$)^{20}Ne reaction

T. R. Wang* and W. Haeberli
Department of Physics, University of Wisconsin, Madison, Wisconsin 53706

S. W. Wissink
Indiana University Cyclotron Facility, Bloomington, Indiana 47405

S. S. Hanna
Department of Physics, Stanford University, Stanford, California 94305

(Received 25 June 1987)

The cross sections and analyzing powers of the ^{19}F($\vec{p},\gamma_0\gamma_1$)^{20}Ne reactions have been measured with high precision at nine angles for 24 incident proton bombarding energies in the range 3.5–13.3 MeV, corresponding to excitation energies in ^{20}Ne of 16.0 to 25.5 MeV. At each energy, the $E1$ and $E2$ transition matrix elements were determined from a partial wave analysis of the angular distributions of γ_0. For excitation energies above 23.5 MeV, the calculated direct capture $E2$ strength can account for most of the measured strength. However, a sizable $E2$ strength in excess of direct capture was measured for $E_\gamma \leq 23.5$ MeV. Our results indicate that $\approx 9\%$ of the isoscalar $E2$ sum rule is exhausted in the (γ_0,p$_0$) reaction for excitation energies from 16.0 to 25.5 MeV. A comparison with (α,α') results shows for the first time essential agreement between $E2$ strengths observed with the two modes of excitation. The analysis of the (p,γ_0) data reveals strong evidence for an $M1$ resonance near an excitation energy of 17.7 MeV. The analysis of angular distribution measurements for the γ_1 decay channel is also reported.

I. INTRODUCTION

The existence and the characteristics of the giant quadrupole resonance (GQR) in light nuclei have long been of interest to nuclear physicists. There is now substantial evidence for the existence of a compact isoscalar GQR in the medium to heavy nuclei,[1] but the experimental evidence in the light nuclei is less clear. For the isovector GQR the situation is unclear for all nuclei. The observed $E2$ strength in the light nuclei is quite fragmented,[1,2] and there is still a question of whether a sizable fraction of the $E2$ sum rule is exhausted in a limited energy range.

The major goal of this work is to measure accurately the $E2$ strength as a function of excitation energy in ^{20}Ne as seen through the ^{19}F(p,γ_0)^{20}Ne reaction channel. For this purpose, the angular distributions of cross sections and analyzing powers of the ^{19}F($\vec{p},\gamma_0$)^{0}Ne reaction were measured with polarized incident protons as a function of proton bombarding energy. From these measurements one is able to determine the structure of the (γ,p$_0$) GQR of ^{20}Ne.

The advantages of using polarized proton capture as a probe to study the relatively weak GQR have long been recognized.[2] In electromagnetic reactions the intensity of $E2$ radiation is usually 1 to 2 orders of magnitude weaker than $E1$ radiation. But in a polarized proton capture reaction the cross section and analyzing power carry information on the $E1$-$E2$ interference. In certain favorable cases, e.g., if $J_{\text{target}}=\frac{1}{2}$, $J_{\text{residual}}=0$ or vice versa, the measurement of the angular distributions of the analyzing power and the cross section allows a unique determination of the magnitudes and the phases of the reaction amplitudes if the $E1$ and $E2$ radiations are the only dominant multipolarities (see Sec. IV).

Recently, considerable $E2$ strength of undetermined isospin character has been found in ^{16}O by means of polarized proton capture[3-7] in a region around $E_\gamma=25$ MeV. The $E2$ strength is not found in the corresponding excitation energy region in hadronic excitation,[8-10] and it is possible that this $E2$ strength may be mainly isovector in character. Unfortunately, similar comparisons of the $E2$ strength for other 4N light nuclei are not available because of the lack of high precision in ($\vec{p},\gamma_0$) measurements and the background problems in the hadronic excitations.[9,10] A goal of the present study is to obtain such a comparison for the interesting case of ^{20}Ne.

The study of $E2$ strength in the ^{20}Ne nucleus provides a crucial testing ground for the characteristics of the GQR in the light nuclei. From experimental[11-13] and theoretical[14] studies of the deformed ^{20}Ne nucleus, it is well known that the giant dipole resonance shows very pronounced doorway structure in the region $E_\gamma=16$–21 MeV, where the cross sections in the peaks and the valleys of the giant $E1$ resonance can change as much as 2 orders of magnitudes in a 1 MeV interval. It is interesting to learn if the GQR in ^{20}Ne also possesses such a pronounced doorway structure.

Kurjan *et al.*[12] used the polarized proton capture reaction as a probe of giant multipole strength in ^{20}Ne. However, the emphasis was on the $E1$ resonance, and the three angle polarization distributions in this work could not provide sufficient precision to lead to definitive conclusions on the nature of the GQR.

In this paper we report angular distribution measurements of cross sections and analyzing powers of the reactions $^{19}F(\vec{p},\gamma_0)^{20}Ne$ and $^{19}F(\vec{p},\gamma_1)^{20}Ne^*$ for 24 incident proton bombarding energies between 3.5 and 13.3 MeV. The statistical accuracy of the present analyzing powers is about five times better than in the previous work,[12] and measurements were made at nine angles rather than three angles. As a by-product of these ground-state capture studies, information was also obtained on the $^{19}F(\vec{p},\gamma_1)^{20}Ne^*$ reaction. However, because of the 2^+ spin of the final state in ^{20}Ne, the analysis is too complicated to provide a determination of the $E1$ and $E2$ strengths in the (p,γ_1) channel in a model-independent manner.

II. EXPERIMENTAL PROCEDURES

The present experiment was conducted with the University of Wisconsin tandem accelerator. Polarized H^- ions for injection into the tandem accelerator were provided by a colliding-beam polarized-ion source.[15] The capture γ rays were detected in a cylindrical NaI(Tl) spectrometer described elsewhere.[6] The measurements covered the angular range from 25° to 155°, and the detector subtended a solid angle of 31.1 msr.

A. Beamline and beam collimation

A schematic diagram of the beamline and the experimental setup is shown in Fig. 1. Between the scattering chamber and the removable beam stop the beamline is lined with a 0.1 cm thick lead sheet to reduce possible neutron and γ-ray backgrounds produced by scattered protons.

The position of the beam on the target is defined by slits 1 and 2. The slit openings are 1.27 cm wide by 1.52 cm high for slit 1, and 1.5 mm by 3.0 mm for slit 2. The currents in the beam steerers are controlled by feedback from the slit signals which keeps the beam centered on the target.

B. Scattering chamber and target

The determination of the $E2$ strength in the $^{19}F(\vec{p},\gamma)^{20}Ne$ reaction requires high precision measurements of the relative cross sections as a function of angle. Hence, the cylindrical scattering chamber and target assembly were designed to minimize possible misalignment between the target beam spot and the axis of rotation of the NaI detector. Tolerances in constructing the assembly were ± 0.05 mm.

The target chamber provides for mounting particle monitor detectors (Si surface barrier detectors) in the reaction plane at a scattering angle of $\theta = 90°$ and symmetrically above and below the reaction plane, $\phi = 90°$ and 270°, at $\theta = 157.5°$. The target, scattering chamber, and beamline beyond the scattering chamber were electrically isolated from ground and served as a Faraday cup. An electron suppressor located behind slit 2 permits accurate current integration.

The fluorine target consisted of a layer of CaF_2 evaporated onto a 50 $\mu g/cm^2$ carbon foil. The target thickness was varied between 250 and 100 keV for proton bombarding energies between 3.5 and 13.3 MeV. Inspection under a microscope showed that the surface of the CaF_1 layer was flat and coplanar with the mounting surface on the target ladder to ± 0.12 mm. An aluminum target ladder accommodates four targets. One edge of each target frame was machined down to a thickness of 0.6 mm in order to minimize the range of angles over which it attenuates the γ rays.

The γ-ray attenuation in the target and target frame was studied as a function of NaI spectrometer angle by measuring the $^{19}F(p,\gamma_0,\gamma_1)$ yields when the NaI detector is rotated through the plane of the target. The attenuation by the target frame is $7.0 \pm 0.5\,\%$ when the plane of the target is along the axis of the NaI detector and decreases rapidly as the NaI detector is moved away from the target plane. For the actual measurements the NaI detector was at least $\pm 10°$ away from the plane of the target frame where the attenuation is negligible.

At the beginning of each running period the scattering

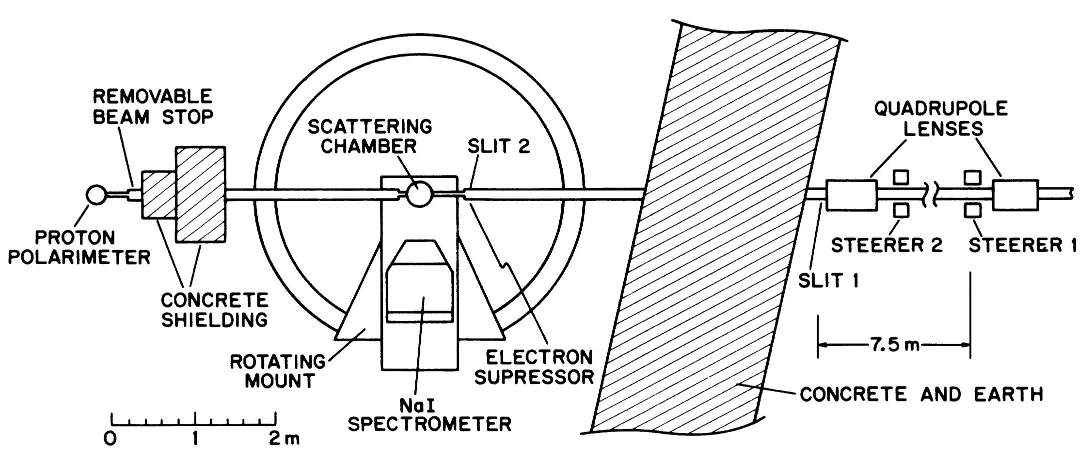

FIG. 1. The configuration of the beamline used in the experiment. The beam direction is from right to left.

chamber was first adjusted to the axis of rotation of the NaI detector to better than $+0.1$ mm. To align the beam spot with the axis of rotation of the target ladder in the direction transverse to the beam, a half target test was made. Slit 1 was shifted transversely until identical proton yields, scattered into the two back angle particle monitors, were detected when a half disk aluminum target was rotated into either the left or right half of the beam. The overall misalignment of the beam spot with respect to the axis of rotation of the NaI detector is less than 0.4 mm in the beam direction and 0.33 mm in the direction transverse to the beam axis. This estimate includes the possible misalignment of the scattering chamber with respect to the NaI detector, of the target ladder with respect to the center of the scattering chamber, and of the axis of rotation of the target ladder with respect to the beam spot on the target. These limits would yield a false anisotropy of the γ-ray angular distribution of $\leq 1\times 10^{-3}$.

As an additional check on the systematic error resulting from possible misalignments, the NaI detector was used to measure the isotropy of γ rays from a ^{56}Co source, produced by activation of a ^{56}Fe target by the proton beam. The γ-ray yields for different target orientations and different detector angles differed from anisotropy by $\leq 2\times 10^{-3}$. Fitting the measured γ-ray angular distribution with a Legendre polynomial series up to order four yielded values of the a_4 coefficient of ≤ 0.002 and for other coefficients ≤ 0.001.

C. Normalization of γ-ray yield

The measured γ-ray yields were normalized by the integrated charge in the Faraday cup (Sec. II B). As a check on possible variation of target thickness during an angular distribution measurement, the alpha particle yields from the ^{19}F(p,α) reaction were measured in the two monitor detectors mounted at $\theta = 157.5°$. The difference in the normalization from total charge integration and particle monitors was $\leq \pm 1\%$ (2%) for 86% (98%) of the data points. Both normalizations were used to extract the angular distribution coefficients and the $E2$ strengths (Sec. IV). The results were essentially identical. The cross sections for the different targets used in the experiment were normalized by the target thickness as determined from the widths of the alpha peaks measured in the particle monitor. The target thicknesses were consistent to $\pm 4\%$ with the relative γ-ray yields at 7.55 MeV, which were measured at the beginning of each running period.

D. Polarization

The data were taken alternately for the two polarization states. The duration and flipping time of each polarization state was 2.5 s and 25 ms, respectively. The beam currents on the target were typically 200 to 450 nA with beam polarizations of $P = 0.80$ to 0.90. An absolute measurement of the proton polarization was made at the beginning and end of each angular sweep by a polarimeter in which p-^{4}He scattering was observed at laboratory angles of $\pm 112.3°$. The analyzing powers ($A \approx 0.9$ to 1.0 for $E_p = 3.5$ to 14.0 MeV) were calculated from the phase shifts reported by Schwandt *et al.*[16] The overall uncertainty of the beam polarization measurements was about 3%, which includes the uncertainties in the calculation of the ^{4}He(p,p)^{4}He analyzing powers and the statistical errors of the beam polarization measurements.

The constancy of the beam polarization was monitored by the ^{19}F($\vec{p}$,p)^{19}F reaction, which has an analyzing power of about 0.2. The beam polarizations were constant within $\pm 0.5\%$ over a typical angular distribution measurement, and varied less than 2% over a seven day running period.

E. NaI detector electronics

The electronics of the NaI detector incorporated both an anticoincidence requirement with the anticoincidence shield and a pileup rejection circuit similar to those of Refs. 6 and 17. The efficiency of rejecting cosmic rays by the anticoincidence electronics was measured to be greater than 98%. The NaI events which pass the pileup rejection electronics, and are in anticoincidence (or coincidence) with plastic scintillator events, were routed into an analog to digital converter (ADC) as an accept (or reject) spectrum. Typical NaI spectra are shown in Fig. 2. The solid lines in the figure show the fitted line shapes (see Sec. III). The pileup rejection and anticoincidence electronics are especially important in this ^{19}F(p,γ) experiment because of the small separation between the γ_0 and γ_1 peaks in the energy spectrum.

To correct for the dead time in the signal processing electronics, a pulser signal, whose frequency is proportional to the beam current, is inserted into the NaI spectrum well above the γ_0 peak, and separately into a scaler. A comparison of the number of pulses recorded in the scaler with the number that pass through the NaI electronics gave dead time corrections of 2–12 % for typical counting rates of 20–120 kHz. In order to minimize errors in dead time and pileup corrections, the NaI counting rate was kept constant during an angular distribution measurement by adjusting the beam current at the target.

III. DATA ACQUISITION AND REDUCTION

The cross sections and analyzing powers of the ^{19}F($\vec{p}$,γ)^{20}Ne reaction were measured for 24 proton bombarding energies in the range 3.5–13.3 MeV. The proton energies were chosen at the peaks and the valleys of the total cross section curve of the ^{19}F(p,γ_0)^{20}Ne reaction for $E_p \leq 7.8$ MeV and in 500 keV steps for $E_p > 7.8$ MeV. For each energy, measurements were made at angles of 25°, 50°, 90°, 130°, 155°, 142.5°, 110°, 70°, and 37.5° with the target plane set at 60° to the beam and then in the reverse order at 155°, 130°, 90°, 50°, 25°, 37.5°, 70°, 110°, and 142.5°, with the target at 120°. This procedure was adopted to detect possible systematic errors such as those due to gain shifts. At the beginning of each running period, the angular distribution measurement at $E_p = 7.55$ MeV was repeated to determine the reproducibility of the experimental setup. The results were reproducible within statistics. The final γ-ray angular distributions were converted to the center-of-mass system and corrected for the effects of the finite detector solid angle.[18] The average statistical errors in the yield at each angle are 1% for γ_0 and for γ_1 and 0.01 in the analyzing powers. The errors are largest in the valleys of the yield curve, where they reach at most about 5% and 0.05 for cross sections and analyzing powers, respectively.

In the observed γ-ray spectra, the γ_0 and γ_1 peaks partially overlap, and a line shape fitting procedure was used to extract the separate yields. Figure 2 shows an example of fitting line shapes to the γ-ray spectra and to the analyzing powers evaluated channel by channel from the spin up and spin down γ-ray spectra.

The γ-ray line shape used consisted of the following components: (i) three identically skewed Gaussians with centroids spaced 511 keV apart, to describe the full-energy, first-escape, and second-escape peaks of the γ-ray response; (ii) an exponential bremsstrahlung tail to the left of the full-energy centroid; and (iii) an exponential tail to the right of the full-energy centroid to represent

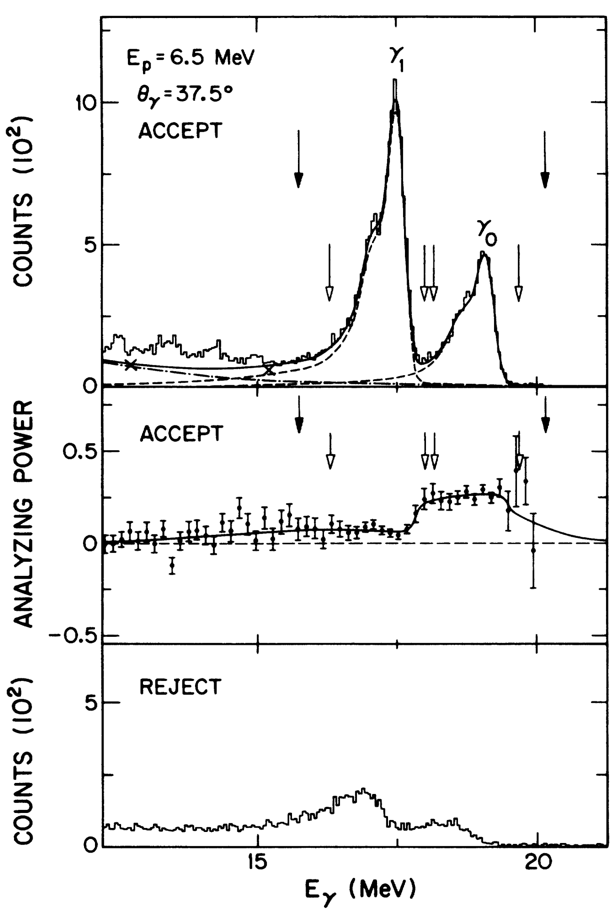

FIG. 2. Typical NaI accept and reject pulse height spectra. The solid lines in the accept spectra are the fits to the overall γ-ray line shapes. The dashed lines are fits to each γ-ray peak and the dot-dashed line is the fitted background. The two crosses in the accept energy spectrum are estimated points of the exponential background (see the text). The solid arrows give the fitting regions and the open arrows the summing windows for γ_0 and γ_1 peaks (see the text). The data points in the analyzing power plot are the average of three adjacent channels.

unsuppressed pileup arising from the intense background of small NaI pulses. The overall background in the peak region is parametrized as a constant cosmic ray background plus an exponential tail which arises from unsuppressed pileup of many low energy events in the detector. The large difference in analyzing powers of the γ_0 and γ_1 peaks greatly facilitated the determination of the tails of the γ-ray line shape, which then constrained the exponential background underneath the γ_0 and γ_1 peaks. To prevent the exponential background outside of the main fitting region (solid arrows in Fig. 2) from being physically unrealistic, the trend of the background outside of the fitting region was estimated as shown by the crosses in Fig. 2.

The line shape and the background parameters were fixed to produce an average curve representing all the measured $^{19}F(\vec{p},\gamma)^{20}Ne$ spectra. Good fits to all γ-ray spectra were obtained with this universal curve, except that allowance was made for an observed slight decrease in relative peak width with increase in γ-ray energy. For the roughly 80 data points in each γ_0 plus γ_1 fit, the average reduced χ^2 varied typically between 1.0 and 1.4 over the runs.

The γ_0 and γ_1 yields were obtained by summing the actual counts in windows of constant percentage width suitably positioned around the γ_0 and γ_1 centroids and subtracting the local background from these sums (see the following). Typical summing windows are shown in Fig. 2. Because the relative separation between γ_0 and γ_1 decreases with increasing proton energies, the chosen widths of the summing regions were reduced appropriately with increasing proton bombarding energy. This caused a change in γ-ray detection efficiency and thus made necessary a correction to the angular integrated yields that changed by $\approx 8\%$ in going from $E_p = 3.5$ MeV to $E_p = 13.3$ MeV.

In the determination of each γ_0 and γ_1 peak sum, the background caused by the tail of the adjacent peak and by the exponential background was subtracted from the actual number of counts in the summing window. In this way of obtaining peak sums the fitted curve is used only to determine the centroids which fix the window locations and widths and the backgrounds to be subtracted from the sums. Thus, the γ yields are based essentially on the actual counts. The quality of the fit within the window is not very important; rather the emphasis is on the correct representation of the background and the tail from the nearby peak. Therefore, the fact that the γ-ray peak is somewhat more sharply peaked than the Gaussian (see Fig. 2) is of little consequence. The uncertainty in the γ-ray yield was taken as the rms sum of the uncertainties in the following quantities: the observed counts within the summing window; the counts corresponding to the background yield within the summing window; and the error in the computation of this background yield.

The average correction to the γ_0 yield from the γ_1 tail is $\approx 2\%$. This introduces a correction to the analyzing power of ≈ 0.01. The correction to the γ_0 peak from background is largest at the highest energy where it is $\approx 13\%$ in the yield and ≈ 0.05 in the analyzing power. On the other hand, the correction to the γ_1 yield from the γ_0 tail changes the yield typically by $\approx 8\%$ and the analyzing power by ≈ 0.03. In some cases, the correction to γ_1 yields is as large as $\approx 20\%$. To estimate the effect on the $E2$ strength for γ_0 due to such uncertainties, the $E2$ strength was calculated for γ_0 peak sums extracted from two extreme cases of the line shape parameters. The results for the worst case ($E_p = 13.3$ MeV), where the corrections to the γ_0 yields are particularly large, indicate that the uncertainty in the $E2$ strength arising from the uncertainty in line shape parameters is less than half the uncertainty due to other sources. Except at the very highest γ-ray energies, where the γ_0 cross sections are very small, the γ_0 yields extracted from the line shape fitting procedure and from simple peak sums of the raw data result in similar $E2$ strengths.

Over the γ-ray energy region studied here the total γ absorption in the NaI crystal does not vary significantly.[19] A comparison of the yields in the accept and reject NaI spectra shows that the NaI detector efficiency varies by less than 3% over the energy region studied here. Hence, no detector efficiency corrections were made in the evaluation of the relative cross sections at different energies.

IV. REACTION ANALYSIS

The procedures for the analysis of angular distributions and the extraction of $E1$ and $E2$ strengths from the cross section and analyzing power measurements are similar to those of Wissink *et al.*[6] In the center-of-mass system, we have[20,21]

$$\sigma(E_\gamma,\theta_\gamma)=A_0(E_\gamma)\left[1+\sum_{k=1}^{2L_{\max}} a_k(E_\gamma)P_k(\cos\theta)\right], \quad (1)$$

$$\sigma(E_\gamma,\theta_\gamma)A(E_\gamma,\theta_\gamma)=A_0(E_\gamma)\sum_{k=1}^{2L_{\max}} b_k(E_\gamma)P_k^1(\cos\theta), \quad (2)$$

where $L_{\max}$ is the angular momentum of the highest multipole considered and

$$A_0(E_\gamma)=\frac{1}{4\pi}\int \sigma(E_\gamma,\theta_\gamma)d\Omega$$

contains the energy dependence of the total cross section.

For the ^{19}F$(\vec{p},\gamma_0)^{20}$Ne reaction, only two complex reaction amplitudes in the proton entrance channel contribute for each γ multipolarity: ${}^1P_1\exp[i\phi({}^1P_1)]$ and ${}^3P_1\exp[i\phi({}^3P_1)]$ for $E1$ radiation, ${}^3S_1\exp[i\phi({}^3S_1)]$ and ${}^3D_1\exp[i\phi({}^3D_1)]$ for $M1$ radiation, and ${}^1D_2\exp[i\phi({}^1D_2)]$ and ${}^3D_2\exp[i\phi({}^3D_2)]$ for $E2$ radiation. The ϕ's denote the phases of these complex reaction matrix elements. If we assume that $E1$ and $E2$ are the only significant multipole radiations involved in the reaction (a major portion of the $M1$ strength is contained in the well-known state[22] at 11.24 MeV), seven parameters (four amplitudes and three relative phases) have to be determined from the nine a_k and b_k coefficients ($L_{\max}=2$) and the system is overdetermined. The expressions for a_k and b_k in terms of the $E1$ and $E2$ reaction matrix elements for the ^{19}F$(\vec{p},\gamma_0)^{20}$Ne reaction are given by Calarco *et al.*[13] The presence of possible $M1$ strength in the ^{19}F$(\vec{p},\gamma_0)^{20}$Ne measurements will be discussed in Sec. V C.

For transitions to the first excited state of ^{20}Ne, the determination of the $E1$ and $E2$ strengths cannot be made in a model-independent manner because the higher angular momentum of the first excited state ($J^\pi=2^+$) allows too many proton partial waves. Thus for the ^{19}F$(\vec{p},\gamma_1)^{20}$Ne reaction, only the angular distribution coefficients and a few remarks are given.

In the first analysis, the angular distributions of γ-ray yields and analyzing powers from each scan were separately fitted to Legendre and associated Legendre polynomials to order four. For each bombarding energy the weighted means of the a_k and b_k coefficients were computed over all angular distribution scans. The entrance channel proton partial wave amplitudes and phases[13] corresponding to $E1$ and $E2$ radiations were then extracted from the averaged a_k and b_k coefficients, and $E1$ and $E2$ strengths were derived. The fitting routine used to extract angular distribution coefficients and $E1$ and $E2$ strengths is similar to that of Wissink *et al.*[6]

In a second analysis, the $E1$ and $E2$ strengths were extracted directly from the experimental values of $\sigma(E_\gamma,\theta_\gamma)$ and $\sigma(E_\gamma,\theta_\gamma)\times A(E_\gamma,\theta_\gamma)$. This procedure has the added advantage that the errors associated with the reduced matrix elements are obtained in terms of experimental errors only, i.e., the propagation of errors through the intermediate calculations need not be considered. The results indicate that the $E2$ strengths and their errors, extracted from the a_k and b_k coefficients or from the σ and $\sigma\times A$ measurements directly, are entirely consistent. In addition, for all bombarding energies, the analyzing powers and relative cross sections measured for the two target angles were consistent within statistical error.

V. RESULTS FOR THE ^{19}F$(\vec{p},\gamma_0)^{20}$Ne REACTION

A. The angular distribution analysis

Typical angular distribution measurements of $\sigma(\theta)$ and $\sigma(\theta)\times A(\theta)$ for the ^{19}F$(\vec{p},\gamma_0)^{20}$Ne reaction and the corresponding polynomial fits (up to order four) are shown in Fig. 3. The reduced χ^2's obtained in the simultaneous polynomial fits of $\sigma(\theta)$ and $\sigma(\theta)\times A(\theta)$ are shown in Fig. 4. A comparison of the distribution of these χ^2 values, with the expected χ^2 distribution for nine degrees of freedom, indicates that a satisfactory fit can be made to all of the angular distributions with $L_{\max}=2$. To verify that the multipole radiations for $L>2$ were negligible (the intensity of $M2$ or $E3$ radiation is usually 1 or 2 orders of magnitude weaker than $M1$ and $E2$ radiations at these energies), the σ and $\sigma\times A$ were fitted to polynomials of order six. The resulting values of the a_5, a_6, b_5, and b_6 coefficients were statistically consistent with zero.

The a_k and b_k coefficients obtained in the polynomial fits are shown in Fig. 5. The solid curve in the total cross section plot is from the previous measurements of Kurjan *et al.*[12] The present measurements are normalized to this curve at one energy (6.5 MeV). The two results are in excellent agreement. For pure $E1$, only A_0, a_2, and b_2

are nonzero. As shown in Fig. 5, the a_1, a_2, and b_1 coefficients are significantly nonzero over the whole energy range, and the a_4 and b_3 coefficients are nonzero at the higher incident proton bombarding energies. These results indicate that radiation other than $E1$ is present.

B. The $E1$ and $E2$ strengths

The reduced χ^2's obtained under the assumption that only $E1$ and $E2$ radiations are present are shown in Fig. 4. The fits to the reaction matrix elements at $E_p=4.8$, 5.2, 5.4, and 5.65 MeV incident proton bombarding energies show anomalously large χ^2's. In view of the good fits to the data with polynomials if $k\leq 4$, we consider these large χ^2's to indicate contributions from $M1$ strength, as will be discussed further in Sec. V C.

The quadratic nature of the system of equations[13] relating the a_k and b_k coefficients to the $E1$ and $E2$ reaction matrix elements introduces two degenerate mathematical solutions for the ampiltudes and phase of the initial proton partial waves. In the LS representation, these two solutions are related to each other by a simple transformation of the phases: $\phi(^3P)\rightarrow\pi-\phi(^3P)$, $\phi(^1D)\rightarrow-\phi(^1D)$, and $\phi(^3D)\rightarrow\pi-\phi(^3D)$. Figure 6 shows the solutions for the proton partial waves which have a negative phase for the ^1D partial wave. The ^1P partial wave has the largest amplitude throughout, as expected, since $E1$ is the dominant radiation in this energy region and the $E1$ (and $E2$) operator to first order (long wavelength approximation[23]) does not flip the spin. The amplitude of the ^1D partial wave is rather constant in the energy region studied here and somewhat larger than the amplitude of the ^3D partial wave.

The absolute and relative cross sections for $E2$ radiation are shown in Fig. 7. There may be correlations between the $E1$ and $E2$ cross sections but this is not clearly established. In any event, the $E2$ strength seems to be highly fragmented into intermediate structures, as is the $E1$ strength, as suggested by the curve that is drawn through the data.

One of the difficulties encountered in extracting the $E2$ strength is the possible presence of multiple minima in χ^2 space. To investigate this, the analysis was repeated with the normalized $E2$ strength constrained to take on successively larger values. Typical results of χ^2 plotted versus the relative amount of $E2$ strength are shown in Fig. 8. Usually, only one χ^2 minimum was found (e.g., see the curve at $E_p=3.5$ MeV). In some cases, a second minimum was found, but at such a large χ^2 (e.g., see 4.1 MeV) that the choice of the proper minimum is straight-

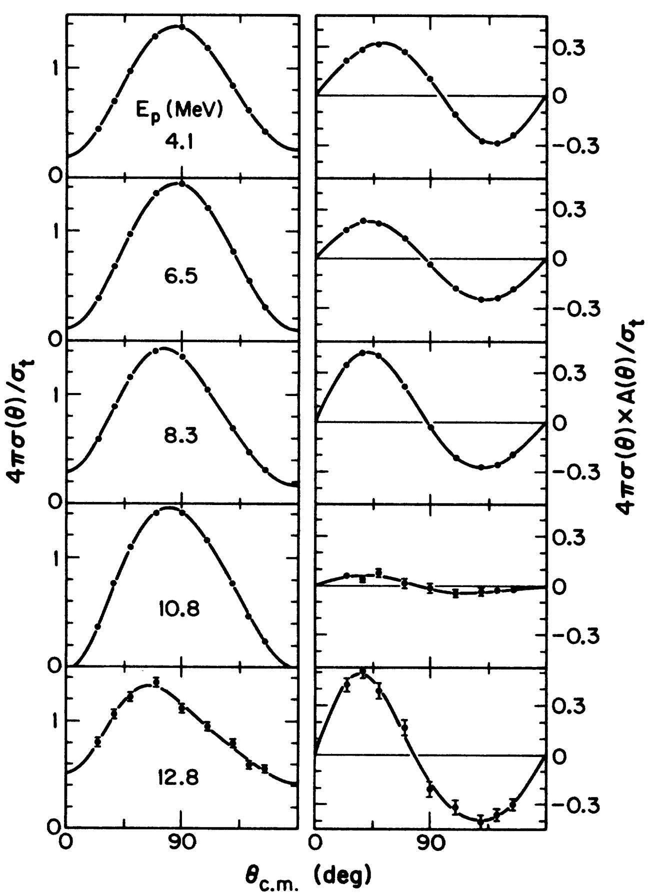

FIG. 3. Representative angular distributions of the $^{19}F(\vec{p},\gamma_0)^{20}Ne$ reaction. The solid curves are simultaneous Legendre and associated Legendre polynomial fits of $\sigma(\theta)$ and $\sigma(\theta)\times A(\theta)$ to order four.

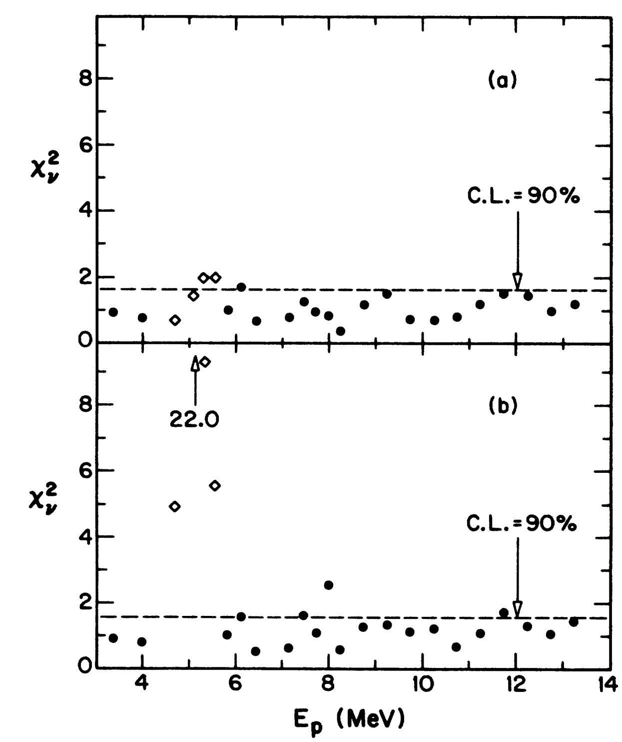

FIG. 4. The normalized χ^2 obtained in fitting $\sigma(\theta)$ and $\sigma(\theta)\times A(\theta)$ measurements of the $^{19}F(\vec{p},\gamma_0)^{20}Ne$ reaction by (a) Legendre and associated Legendre polynomials to order four and (b) reaction matrix elements of $E1$ and $E2$ radiations. The 22.0 value is the normalized χ^2 at $E_p=5.2$ MeV. The diamonds in (a) and (b) are points with poor $E1$ and $E2$ fits. The dashed lines correspond to 90% confidence levels.

forward. However, at 8.8, 11.3 (see Fig. 8), and 13.3 MeV, two χ^2 minima occur in a region of a broad χ^2 minimum. Hence, at these energies the error in the $E2$ strength was determined by the change in $E2$ strength necessary to increase χ^2 by unity from its minimum value.

C. Contributed from $M1$ radiation

As mentioned earlier, there is evidence for $M1$ radiation at four points around 5.2 MeV incident proton energy (see Fig. 4). A unique determination of $M1$ strength cannot be made if both $E1$ and $E2$ radiations are also present, since then 11 reaction matrix elements (six amplitudes and five relative phases) would have to be extracted from the nine a_k and b_k coefficients and the problem is underdetermined.

From angular correlation theory the $M1$-$E1$ interference contributes only to the a_1 and b_1 coefficients, whereas $E1$-$E2$ interference contributes to a_1, b_1, a_3, and b_3. In order to estimate the effect of possible $M1$ contributions on the determination of $E2$ strength throughout, the change in the $E2$ (and $E1$) strength extracted from the a_k and b_k coefficients was calculated when the a_1 and b_1 coefficients were omitted. This would appear to be a valid procedure as long as the $M1$ strength is not large enough to contribute significantly to a_2 and b_2. The change in $E2$ strength was found to be statistically consistent with zero except for the very same energy region (4.8 to 5.65 MeV) where the fits to σ and $\sigma \times A$ were poor. Hence, we conclude the effect of possible $M1$ contributions on the determination of $E2$ strength is negligible except at the points at 4.8, 5.2, 5.4, and 5.65 MeV. The $E2$ reaction matrix elements and strengths plotted at these four points in Figs. 6 and 7 are the values extracted from the a_k and b_k coefficients excluding the a_1 and b_1 coefficients.

In order to estimate the lower limit of the $M1$ strength, the χ^2 of the fit to σ and $\sigma \times A$ was calculated as a function of constrained $^3S_1$ and $^3D_1$ amplitudes of $M1$ radiation. The minimum $M1$ strength required to fit the data

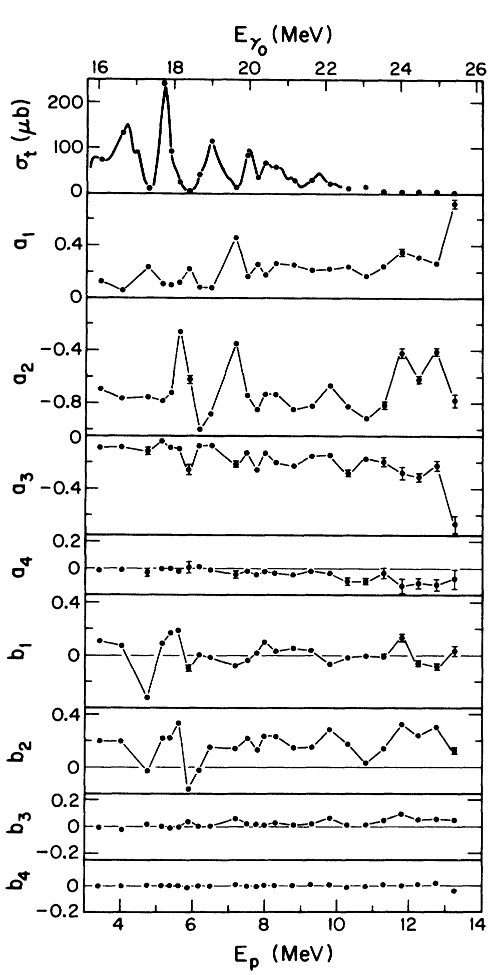

FIG. 5. The polynomial expansion coefficients, a_k and b_k, of the ^{19}F($\vec{p},\gamma_0$)^{20}Ne reaction. The solid curve in the σ_t plot is from the previous measurement of Kurjan *et al.* (Ref. 12). The two measurements are normalized to each other at $E_p = 6.5$ MeV. The solid lines in the a_k and b_k data are connections of adjacent points and have no theoretical meaning.

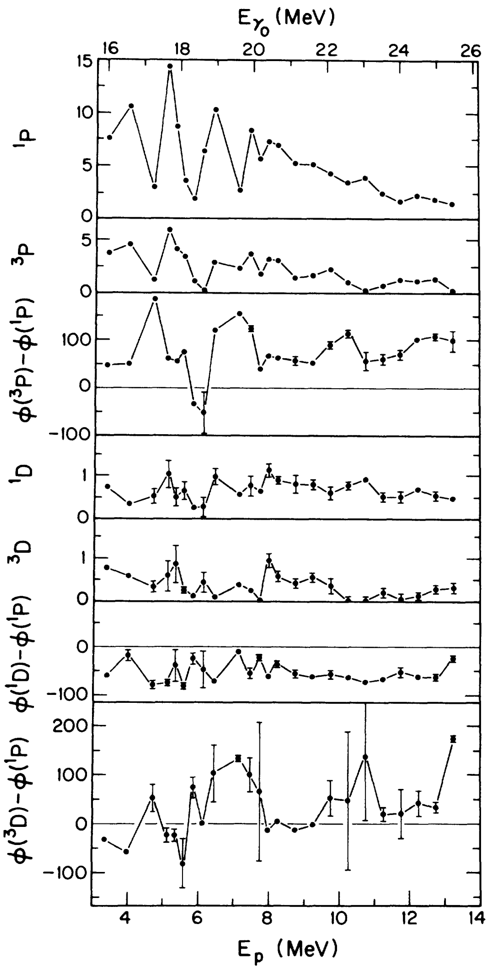

FIG. 6. The entrance channel proton partial wave amplitudes and phases of $E1$ and $E2$ radiations for the ^{19}F($\vec{p},\gamma_0$)^{20}Ne reaction. Only the solution with negative ^1D phases is presented. The units of the partial wave amplitudes and phases are $(\mu b)^{1/2}$ and deg, respectively. The solid lines are connections of adjacent points and have no theoretical meaning.

at 5.2 MeV ($E_\gamma = 17.7$ MeV), where the $M1$ strength produces the largest effect, is 0.92 μb. In order to deal with this $M1$ strength, we assume it to be represented by a Breit-Wigner resonance with a total width of 0.5 MeV. Since the ground state proton decay width is less than the total width, we estimate the $M1$ radiative decay width and strength $B(M1)$ to be ≥ 0.62 eV and $\geq 9.7\times10^{-3}\,\mu_0^2$, respectively, where μ_0 is the nuclear magneton. This transition strength amounts to $\geq 1.5\%$ of the $M1$ transition strength for the $M1$ level at 11.24 MeV as found from 180° electron scattering.[22]

D. Direct capture calculation

Here we investigate the amount of the observed $E2$ strength that could be caused by direct capture,[24,25] since it is only the excess strength that should be assigned to a GQR. The direct capture $E2$ cross section in the long wavelength limit can be derived from Eqs. (10)–(13) of Ref. 24. In the present calculation, the initial-state distorted wave function was calculated with an optical model potential, whereas the final bound-state single-particle wave function was obtained from the real part of the optical model potential with the depth of the potential adjusted to reproduce the known bound-state energy. The optical potential parameters proposed by Watson *et al.*[26] for $1p$ shell nuclei were used. Both continuum and bound-state wave function calculations were carried out with the program PTOLEMY.[27] To check the calculation, the direct capture $E2$ cross section calculation of the $^{15}N(p,\gamma_0)^{16}O$ reaction was compared with previous calculations.[7,28]

To compare with the measured $E2$ strength, the calculated direct capture $E2$ strength must be multiplied by the photon spectroscopic factor, C^2S (Ref. 29). The value used for $^{19}F + p \rightarrow {}^{20}Ne$, $C^2S=0.36$, is the average of two measurements:[30,31] $C^2S=0.43$ and $C^2S=0.30$. The result is shown as a function of energy in Fig. 7. The cross section varies from ≈ 0.09 μb at $E_\gamma = 16$ MeV, to ≈ 0.38 μb at $E_\gamma = 26$ MeV. We note that above $E_\gamma = 23$ MeV, the calculated $E2$ direct capture cross section accounts for most of the measured $E2$ strength, while in the energy region 16 to 23 MeV, a sizable amount of $E2$ strength in excess of the direct capture cross section is found.

E. Sum rule estimate

For $E2$ photoexcitation the appropriate isoscalar energy weighted sum rule (EWSR) is almost model independent[4,32] and reduces to

$$\int \frac{\sigma}{E^2}dE = 2.55\times10^{-5}\frac{Z^2}{A}\langle R^2\rangle \ \mathrm{MeV}^{-1}\,, \tag{3}$$

where the nuclear charge and mass number, Z and A, are dimensionless, the excitation energy E is in MeV, and σ

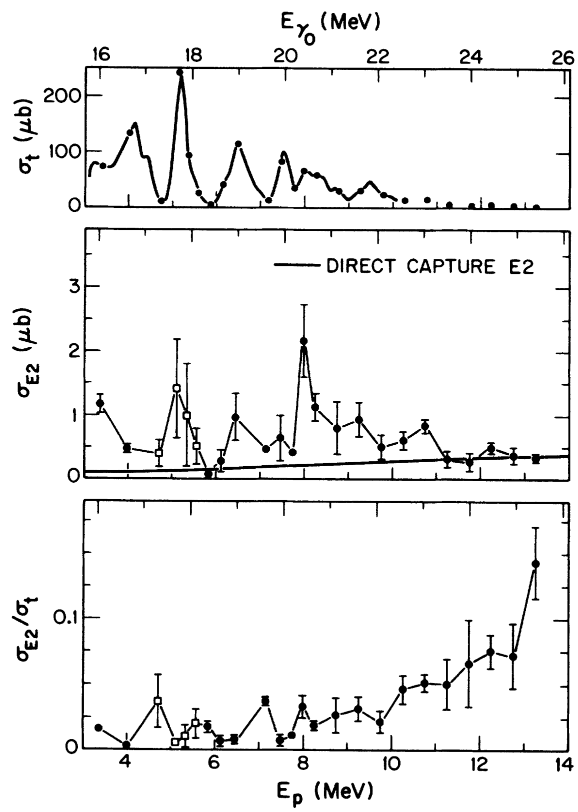

FIG. 7. The cross sections and relative cross sections of $E2$ strength for the $^{19}F(\vec{p},\gamma_0)^{20}Ne$ reaction. Where no error bars are shown, the error is smaller than the size of the point. The square points around $E_p = 5.2$ MeV are from the fitting of reaction matrix elements to the polynomial expansion coefficients without a_1 and b_1 coefficients. The continuous solid curve in the $E2$ cross section plot is the calculation of direct capture $E2$.

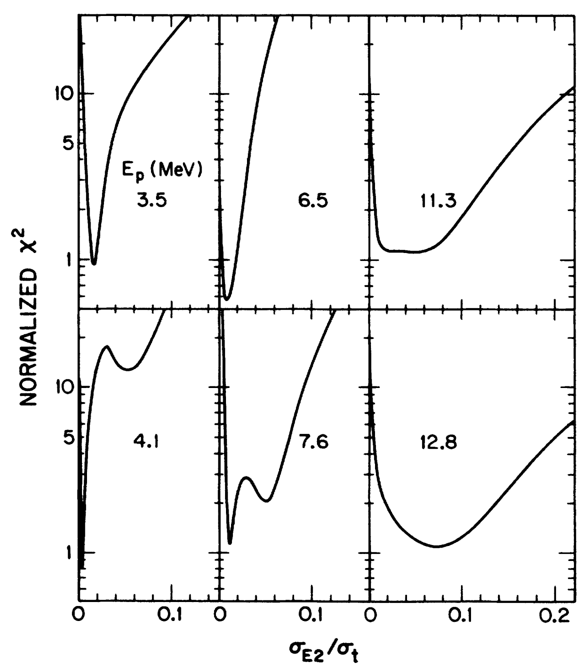

FIG. 8. Representative normalized χ^2 curves vs constrained relative cross sections of the $E2$ strength for the $^{19}F(\vec{p},\gamma_0)^{20}Ne$ reaction. The increment of the relative $E2$ cross section is 0.002.

and $\langle R^2 \rangle$, the mean square nuclear charge radius, are in the same units. If we use $\langle R^2 \rangle^{1/2} = 3.00$ fm for ^{20}Ne, as determined from electron scattering data,[33] the isoscalar EWSR amounts to 11.5 μb/MeV. For self-conjugate nuclei, the isovector $E2$ EWSR is the same as the isoscalar $E2$ EWSR, although the isospin dependence of the nuclear potential increases the model dependence of the isovector EWSR.[34]

The $E2$ strength measured in the (p,γ_0) reaction was converted into $E2$ strength in the (γ,p$_0$) reaction by detailed balance.[6] The integrated energy weighted $E2$ strength from $E_\gamma \approx 16.0$ to 25.5 MeV is 0.99 ± 0.09 μb/MeV, which is 8.6 ± 0.8 % of the isoscalar $E2$ EWSR. This value for the (γ,p$_0$) channel is typical not only of other GQR's but also of GDR's in the light nuclei. Thus, the concentration of $E2$ strength appears to represent a giant resonance.

VI. RESULTS FOR THE ^{19}F($\vec{p}$,γ_1)^{20}Ne* REACTION

A few typical angular distribution measurements of $\sigma(\theta)$ and $\sigma(\theta) \times A(\theta)$ for the ^{19}F($\vec{p}$,γ_1)^{20}Ne reaction along with the polynomial fits (up to order four) are shown in Fig. 9. The fits are quite satisfactory since the distribution of the χ^2 values is consistent with the one expected for nine degrees of freedom. As for γ_0 it was shown that multipole radiations higher than $L=2$ could be neglected in fitting the data.

The a_k and b_k coefficients obtained in the polynomial fits are shown in Fig. 10. The solid curve in the total cross section plot is from the previous measurements of Kurjan *et al.*[12] The two sets of data, which were normalized together at 6.5 MeV, are in excellent agreement. As seen in Fig. 10, the a_1, a_3, and b_1 coefficients are significantly nonzero, which indicates that radiation other than $E1$ is present.

One of the significant features of the ^{19}F($\vec{p}$,γ_1) reaction is that the analyzing powers, i.e., the b_k coefficients, are much smaller than in the ^{19}F($\vec{p}$,γ_0) reaction. Also, the a_2 coefficients in the ^{19}F($\vec{p}$,γ_1) reaction are on the average a factor of 2 smaller than in the ^{19}F($\vec{p}$,γ_0) reaction so that the angular distributions of the ^{19}F($\vec{p}$,γ_1) reaction no longer resemble the "typical" $\sin^2\theta$ shape. We attribute these features to greater complexity of ^{19}F($\vec{p}$,γ_1). As mentioned in Sec. IV, it is not possible to extract $E1$ and

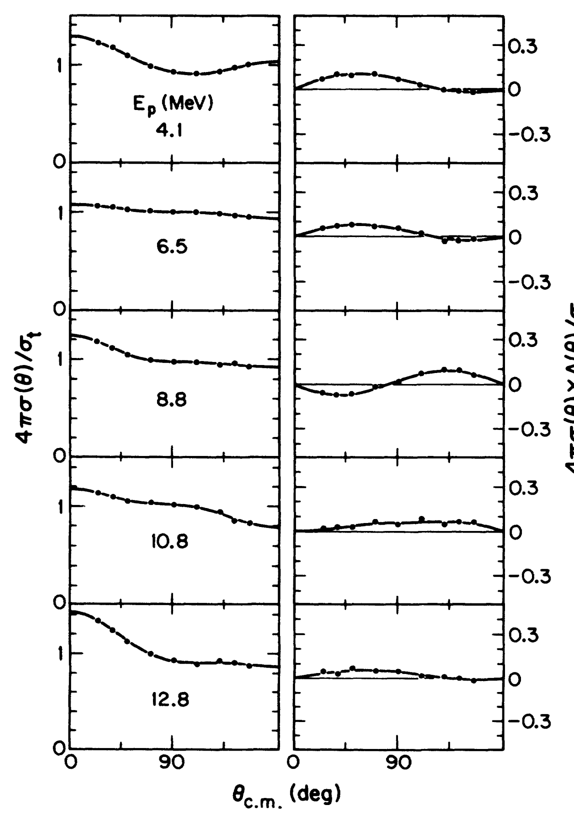

FIG. 9. Representative angular distributions of the ^{19}F($\vec{p}$,γ_1)^{20}Ne* reaction. The solid curves are simultaneous Legendre and associated Legendre polynomial fits of $\sigma(\theta)$ and $\sigma(\theta) \times A(\theta)$ to order four.

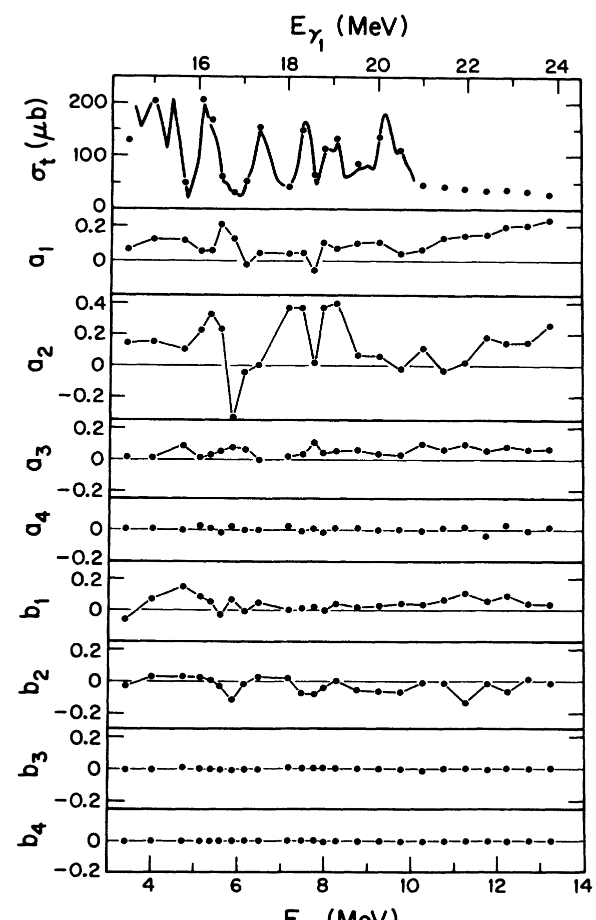

FIG. 10. The polynomial expansion coefficients, a_k and b_k, for the ^{19}F($\vec{p}$,γ_1)^{20}Ne* reaction. The solid curve in the σ_t plot is from the previous measurement of Kurjan *et al.* (Ref. 12). The two measurements are normalized to each other at $E_p = 6.5$ MeV. The solid lines in the a_k and b_k data are connections of adjacent points and have no theoretical meaning.

$E2$ strengths for the $^{19}F(\vec{p},\gamma_1)^{20}Ne$ reaction in a model-independent manner.

VII. OTHER WORK

The $E2$ strength in ^{20}Ne has been excited by inelastic α scattering.[8–10] The results are compared with the photonuclear case in Fig. 11. A comparison of the sum rule strengths is difficult because of the background problems and incomplete separation of various multipole strengths in the hadronic excitation.[1,9,10] In general, the major $E2$ strength occurs at about the same place in the (p,γ_0) and (α,α') measurements. There may also be some correlation of structure as suggested by the arrows in the figure. If 35% of the $E2$ sum rule is exhausted in the (α,α') excitation of the $E2$ resonance, and 20% of its decay is into the p_0, p_1, and p_2 channels[9,10] (see Fig. 11), then this proton decay is of the same order of magnitude as the strength in the p_0 decay channel alone in the present work. However, the energy distribution of the proton decay is very different in the two experiments. Following the (α,α') excitation, the proton decay is broad and featureless, whereas in the (p,γ_0) process it is concentrated into the GQR.

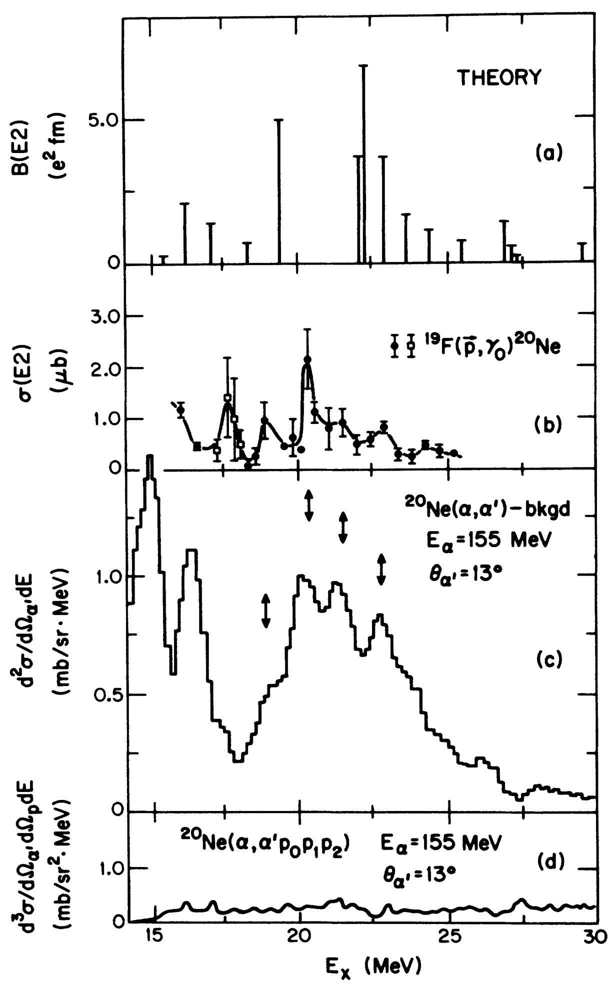

FIG. 11. Comparison of $E2$ strength from this experiment with other work: (a) calculation with the angular momentum projected, deformed particle hole model with Woods-Saxon potential (Ref. 36); (b) the (p,γ_0) reaction, present data, same as Fig. 7; (c) the inelastic (α,α') excitation (Ref. 8); (d) the $(\alpha,\alpha',p_0p_1p_2)$ coincidence process (Refs. 9 and 10).

In the comparison of $E2$ strengths from the two reactions one should keep in mind that the (p,γ_0) reaction is sensitive to both isoscalar and isovector strength, whereas (α,α') excites only the isoscalar part. However, this consideration does not appear to be important in the present comparison since little additional $(T=1)$ strength appears in the (p,γ_0) reaction. This comparison of $E2$ strengths from photoexcitation and hadronic excitation is noteworthy in that it is the first time essential agreement has been observed between the two modes of excitation.[4]

The ^{20}Ne nucleus is an open shell nucleus and presents well-known difficulties in the calculation of giant multipole resonances. In one attempt to overcome these difficulties[35] the low-lying excited states of the valence nucleons in the open-core nucleus ^{20}Ne were coupled to the giant $E0$, $E2$, and $E4$ resonances of the ^{16}O core. This procedure introduces splitting of the giant $E2$ strength in a natural way and may account for some of the structure seen in the $E2$ resonance. Core excitation is thought to be an important feature of some observed giant resonances. Although reasonable agreement with the location of the GQR is obtained with this model, the predicted structure does not appear to be as rich as that observed experimentally.

A more complete and microscopic approach is represented by the deformed particle hole model with angular momentum projected wave functions.[36] The results of such a calculation in a Woods-Saxon potential are shown at the top of Fig. 11. It can be seen that the location of the $E2$ strength and the character of the structure are quite well reproduced by the calculation. Also, in the region 16–28 MeV a sum rule strength of 24% or 34% is predicted for a Woods-Saxon or harmonic oscillator potential, respectively,[36] in good qualitative agreement with the (α,α') result.

We note with interest that Ref. 36 also predicts a weak $M1$ $(T=1)$ level at 14.7 MeV that could be indicative of the $M1$ strength seen in our work. Although the observed energy is 17.7 MeV, we note the theory also predicts the dominant $M1$ level to be at 9.7 MeV, which is also below the observed state at 11.2 MeV.

VIII. CONCLUSIONS

In this work, we have performed precise angular distribution measurements on the photons emitted in the decays to the ground and first excited states of ^{20}Ne following polarized proton capture by ^{19}F. The transition matrix elements in the entrance channel, and therefore the $E1$ and $E2$ strengths of the γ_0 decay channel, have been deduced in a model-independent manner, provided these are the only multipolarities contributing significantly to the reaction. Because of the greater number of spin possibilities in the γ_1 decay channel, the $E1$ and $E2$ strengths cannot be separated uniquely.

In the region studied from $E_\gamma \approx 16.0$ to 25.5 MeV, the $E1$ strength is dominant, with the $E2$ cross section varying from about 2% of the total cross section at $E_\gamma \approx 18$ MeV to about 10% at $E_\gamma \approx 25$ MeV. Around $E_\gamma \approx 17.7$ MeV the analysis shows definite evidence for an $M1$ resonance. Although the absolute width and strength of this resonance cannot be uniquely determined, the study reveals the minimum radiative width and strength to be 0.62 eV and $9.7\times10^{-3}\ \mu_0^2$, respectively. This $M1$ strength is $\geq 1.5\%$ of the strength of the dominant $M1$ level in ^{20}Ne at $E_\gamma = 11.24$ MeV.

The energy weighted $E2$ strength observed in ^{20}Ne(γ,p$_0$)^{19}F, integrated from $E_\gamma \approx 16.0$ to 25.5 MeV, is 0.99 ± 0.09 μb/MeV, which is 8.6 ± 0.8 % of the isoscalar $E2$ EWSR. Up to $E_\gamma = 23.5$ MeV the measured $E2$ strength is on the average a factor of 4 larger than the direct capture cross section. Thus, the observed $E2$ strength cannot be interpreted as arising from a calculated direct capture process.

The $E2$ strength of ^{20}Ne seems to be highly fragmented into intermediate structure in a manner similar to the $E1$ strength. Indeed the structures in the $E1$ and $E2$ resonances may be correlated to some extent, which would suggest a common origin such as the deformation splitting suggested by Schmid and Do Dang[14,36] to explain the $E1$ structure. On the other hand, the core excited model of Knüpfer *et al.*[35] also gives a fairly satisfactory account of the $E2$ structure and is presumably characteristic of a specific multipole. It would be highly instructive to carry out a full doorway-state calculation with wave functions derived from these models.

ACKNOWLEDGMENTS

We wish to thank Professor Claus Rolfs for providing us with a separate calculation of the direct capture $E2$ cross section. We also acknowledge Dr. Steve Mellema for discussions regarding the line shape fitting program. This work was supported by the U.S. National Science Foundation at all three participating universities.

---

*Present address: W. K. Kellogg Radiation Laboratory, California Institute of Technology, Pasadena, CA 91125.

[1]F. E. Bertrand, Nucl. Phys. **A354**, 129c (1981).
[2]H. F. Glavish, S. S. Hanna, R. Avida, R. N. Boyd, C. C. Chang, and E. Diener, Phys. Rev. Lett. **28**, 766 (1972).
[3]H. F. Glavish, in *Proceedings of the Fourth International Symposium on Polarization Phenomena in Nuclear Reactions, Zürich, 1976,* edited by W. Grüebler and V. König (Birkhaüser Verlag, Basel, 1976), p. 317.
[4]S. S. Hanna, in *Photonuclear Reactions I,* Vol. 61 of *Lecture Notes in Physics,* edited by S. Costa and C. Shaerf (Springer-Verlag, Berlin, 1976), p. 275.
[5]K. A. Snover, in *Polarization Phenomena in Nuclear Physics—1980 (Fifth International Symposium, Santa Fe),* Proceedings of the Fifth International Symposium on Polarization Phenomena in Nuclear Physics, AIP Conf. Proc. No. 69, edited by G. G. Ohlsen, R. E. Brown, N. Jarmie, W. W. McNaughton, and G. M. Hale (AIP, New York, 1981), p. 321.
[6]S. W. Wissink, S. S. Hanna, D. G. Mavis, and T. R. Wang, Phys. Rev. C **37**, 2289 (1988), this issue.
[7]J. E. Bussoletti, Ph.D. thesis, University of Washington, 1978.
[8]K. T. Knöpfle, G. J. Wagner, A. Kiss, M. Rogge, C. Mayer-Böricke, and Th. Bauer, Phys. Lett. **64B**, 263 (1976).
[9]K. T. Knöpfle, in *Nuclear Physics with Electromagnetic Interactions,* Vol. 108 of *Lecture Notes in Physics,* edited by H. Arenhövel and D. Drechsel (Springer-Verlag, Berlin, 1979), p. 311.
[10]G. J. Wagner, in *Giant Multipole Resonances,* Proceedings of the Giant Multipole Resonance Topical Conference, Oak Ridge, 1979, edited by F. E. Bertrand (Harwood Academic, Chur, 1980), p. 251.
[11]R. E. Segel, Z. Vager, L. Meyer-Schützmeister, P. P. Singh, and R. G. Allas, Nucl. Phys. **A93**, 31 (1967).
[12]P. M. Kurjan, J. R. Calarco, G. A. Fisher, and S. S. Hanna, Phys. Rev. C **37**, 2281 (1988), this issue.
[13]J. R. Calarco, P. M. Kurjan, G. A. Fisher, and S. S. Hanna, Phys. Lett. **92B**, 67 (1980). A misprint occurs in this reference. The coefficient of the last term in σa_3 should be 1.549, not 1.49. This misprint does not occur in Ref. 12.
[14]K. W. Schmidt and G. Do Dang, Z. Phys. A **276**, 233 (1976); Phys. Lett. **66B**, 5 (1977); Phys. Rev. C **15**, 1515 (1977).
[15]W. Haeberli, M. D. Barker, C. A. Gossett, D. G. Mavis, P. A. Quin, J. Sowinski, T. Wise, and H. F. Glavish, Nucl. Instrum. Methods **196**, 319 (1982).
[16]P. Schwandt, T. B. Clegg, and W. Haeberli, Nucl. Phys. **A163**, 432 (1971).
[17]E. M. Diener, J. F. Aman, S. L. Blatt, and P. Paul, Nucl. Instrum. Methods **83**, 115 (1970).
[18]M. E. Rose, Phys. Rev. **91**, 610 (1953).
[19]M. Suffert, W. Feldman, J. Mahieux, and S. S. Hanna, Nucl. Instrum. Methods **63**, 1 (1968).
[20]J. M. Blatt and L. C. Biedenharn, Rev. Mod. Phys. **24**, 258 (1952).
[21]A. Simon, Phys. Rev. **92**, 1050 (1953).
[22]L. W. Fagg, Rev. Mod. Phys. **47**, 683 (1975).
[23]S. A. Moszkowski, in *Beta- and Gamma-Ray Spectroscopy,* edited by K. Siegbahn (North-Holland, Amsterdam, 1955), p. 373.
[24]R. F. Christy and I. Duck, Nucl. Phys. **24**, 89 (1961).
[25]T. A. Tombrello and P. D. Parker, Phys. Rev. **131**, 2582 (1963).
[26]B. A. Watson, P. P. Singh, and R. E. Segel, Phys. Rev. **182**, 977 (1969).
[27]M. H. Macfarlane and S. C. Pieper, Argonne National Laboratory Report ANL-76-11, 1976, Revision 1.
[28]C. Rolfs (private communication).
[29]C. Rolfs, Nucl. Phys. **A217**, 29 (1973).
[30]A. W. Obst and K. W. Kemper, Phys. Rev. C **8**, 1682 (1973).
[31]H. M. Sen Gupta, T. A. Belote, and D. Roaf, Nucl. Phys. **A267**, 205 (1976).
[32]M. Gell-Mann and V. L. Telegdi, Phys. Rev. **91**, 169 (1953).
[33]C. W. De Jaeger, H. De Vries, and C. De Vries, At. Data Nucl. Data Tables **14**, 479 (1974).
[34]G. R. Satchler, Phys. Rep. **14**, 97 (1974).
[35]W. Knüpfer, W. K. Knauss, and M. G. Huber, Phys. Lett. **66B**, 305 (1977).
[36]K. W. Schmid, Phys. Rev. C **24**, 1283 (1981).